Effective property evaluation and analysis of three-dimensional periodic lattices and composites through Bloch-wave homogenization

Ganesh U. Patil, and Kathryn H. Matlack

Citation: The Journal of the Acoustical Society of America **145**, 1259 (2019); doi: 10.1121/1.5091690
View online: https://doi.org/10.1121/1.5091690
View Table of Contents: https://asa.scitation.org/toc/jas/145/3
Published by the Acoustical Society of America

Effective property evaluation and analysis of three-dimensional periodic lattices and composites through Bloch-wave homogenization

Ganesh U. Patil and Kathryn H. Matlack[a)]
Department of Mechanical Science and Engineering, University of Illinois Urbana-Champaign, Urbana, Illinois 61801, USA

(Received 22 August 2018; revised 10 January 2019; accepted 1 February 2019; published online 6 March 2019)

Periodic lattices offer enhanced mechanical and dynamic properties per unit mass, and the ability to engineer the material response by optimizing the unit cell. Characterizing the effective properties of these lattice materials through experiments can be a time consuming and costly process, so analytical and numerical methods are crucial. Specifically, the Bloch-wave homogenization approach allows one to characterize the effective static properties of the lattice while simultaneously analyzing wave propagation properties such as band gaps, propagating modes, and wave directionality. While this analysis has been used for some time, a thorough study of this approach on three-dimensional (3D) lattice materials with different symmetries and geometries is presented here. Bloch-wave homogenization is applied to extract the effective stiffness tensor of 3D periodic lattices and confirmed with elastostatic homogenization, both within a finite element framework. Multiple periodic lattices with cubic, transversely isotropic, and tetragonal symmetry, including an auxetic geometry, over a wide range of relative densities are analyzed. Further, this approach is used to analyze 3D periodic composite structures, and a way to tailor their overall anisotropy is demonstrated. This work can serve as the basis for nondestructive evaluation of metamaterials properties using ultrasonic velocity measurements.
https://doi.org/10.1121/1.5091690

[BA] Pages: 1259–1269

I. INTRODUCTION

Periodic lattice materials contain spatial repetitions of a unit cell comprised of trusses connected in a specific geometry or configuration. These lattice materials possess better mechanical properties per unit mass compared to their parent bulk material[1] and the geometric periodicity of these structures often regulates their static, dynamic, and wave propagation properties.[2] Due to their unusual properties, lattice materials have potential applications as structural components (high strength-to-weight ratios),[3] for enhanced energy absorption (impact mitigation ability),[4–6] and biomaterials.[7] The performance of lattice materials strongly depends on their effective properties, thus evaluating these properties is essential but at the same time not quite straightforward, specifically when the structure includes complexity in the form of symmetry and geometry. Further, for these lattice materials to be adopted in structural components and applications, methods of nondestructively evaluating their properties and degradation over operation are critical.

There have been many efforts in past years to develop methodologies to evaluate lattice effective properties. For example, the effective mechanical properties of two-dimensional (2D) honeycomb and foam structures have been evaluated analytically by Gibson and Ashby[1] and of a three-dimensional (3D) octet lattice by Deshpande *et al.*[8] In initial analytical evaluations, lattice trusses were modeled as slender bars to study axial deformation, or as Euler-Bernoulli and Timoshenko beams to study bending deformation.[1,8] These assumptions limit the application of the theory to small relative densities. Later work by Chen[9] incorporated bending as well as twisting deformation of 2D honeycomb cells using the generalized variational principle to accurately model flexural rigidity. To study the effects of height of the 2D honeycomb, Hohe and Becker[10] used a strain energy based analytical method to evaluate the stiffness tensor. Even though there has been a significant improvement in analytical methods for lattice effective property evaluation, their use remains limited as it becomes difficult to apply them on complex 3D geometries over a wide range of densities.

To overcome the limitations and narrow feasibility band of analytical methods, finite element (FE) modeling has been explored. Scarpa *et al.*[11] considered 2D auxetic honeycomb structure with negative in-plane Poisson's ratio. They evaluated uniaxial Young's modulus and Poisson's ratio through static FE by considering two-node beam elements for each truss. Wallach and Gibson[12] also used the static FE approach to evaluate the moduli of 3D structures of various aspect ratios, by modeling them as spring and truss elements while incorporating periodic boundary conditions. They considered an orthotropic lattice with nine independent constants that needed six independent simulations for the stiffness tensor evaluation. This same process has been extended by Dalaq *et al.*,[13] to evaluate the effective properties of triply periodic

a)Electronic mail: kmatlack@illinois.edu

minimal surfaces (TPMS) but without beam modeling. The limitation with the use of static FE simulation is its demand for the higher number of simulations for anisotropic structures.

Wave propagation methods can simultaneously extract static effective properties and wave propagation properties of a material, condensing the computation time. Elsayed and Pasini[14,15] used the Bloch-wave method in conjunction with the Cauchy-Born hypothesis (collectively called "Bloch-wave homogenization" hereafter) to obtain the stiffness of 2D lattices with a pin and rigid jointed architectures. Phani *et al.*[2] also used the Bloch-wave homogenization method for 2D isotropic lattices such as triangular, hexagonal, and kagome, by modeling the trusses as Timoshenko beams. Their work was extended to anisotropic topologies by Chopra[16] and Lie *et al.*[17] but was restricted to planar structures. Krodel *et al.*[18] applied this same method to a 3D anisotropic auxetic lattice using one-dimensional (1D) Timoshenko beam elements connected by rigid joints. Even though the wave propagation method has been around for some time, its use for effective property evaluation has not yet been fully applied and studied, specifically for 3D lattices. Modeling 3D lattices in an FE framework with 3D truss elements and without rigid joint assumptions is of prime importance in order to simulate more realistic deformations of lattice materials. For the efficient use of this approach in the design process, the wave propagation method needs to be validated on different geometries having higher anisotropy. There also exists few other methods for evaluation of effective properties such as asymptotic homogenization[19] (specifically for heterogeneous structures), homogenization based on the equation of motion,[19] and dynamic equivalent continuum model[20] (incorporating microinertial effect of low density lattices) that have their own advantages and limitations but are beyond the discussion of this article. Further, researchers working in the field of nondestructive evaluation have explored wave propagation in anisotropic materials to predict quality (or condition) of the material through experimentally evaluated wave velocities.[21–23] However, applying this method to instead obtain the material properties of 3D periodic lattice materials from wave velocities has not yet been fully explored.

In this article, we outline in detail the Bloch-wave homogenization method for effective stiffness tensor evaluation of 3D periodic lattices with different geometries, anisotropies, and densities. The lattices of interest are cubic,[24] foam, octet,[25] and Kelvin[24,25] of cubic symmetry; hexagonal[2] of transversely isotropic symmetry; and a modified octet (termed "octet-A") and bowtie[26] of tetragonal symmetry. We present an in-depth analysis of the bowtie lattice, and the way its wave velocities and effective properties evolve over a range of internal cell angle, α, [Fig. 1(e)] that cause the lattice to vary from negative to positive Poisson's ratio. We extend this method to analyze periodic lattices embedded in a second solid material, referred to as "composite structures." We manipulate these composite structures in terms of their geometry, truss thickness, and bulk material properties to obtain variations in their elastic properties and anisotropy. The organization of this paper is as follows: Sec. II briefly explains the different lattices under consideration.

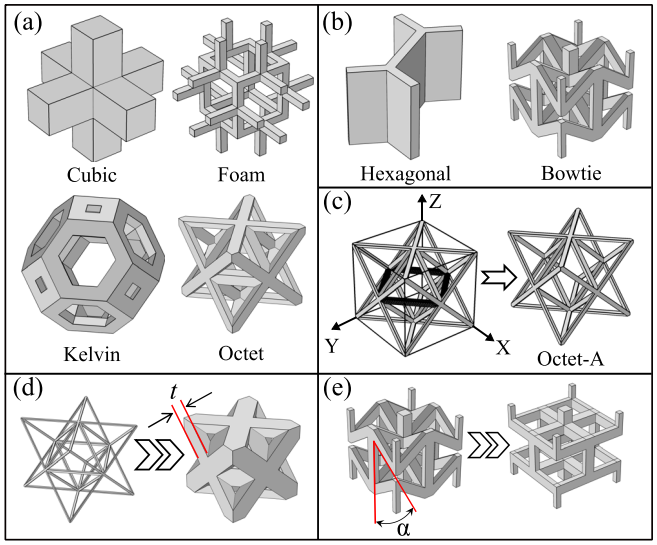

FIG. 1. (Color online) Unit cells of (a) cubic symmetry lattices and (b) lower symmetry lattices. (c) Transformation of cubically symmetric octet lattice into a tetragonal "octet-A" lattice by removing four trusses (highlighted in black). The coordinate system shown is used for all unit cell configurations. The effect of lattice geometry parameterization is shown for (d) truss thickness, t, of octet lattice and (e) internal cell angle, α, of bowtie lattice.

Sections III and IV review the elastostatic and Bloch-wave homogenization theories, respectively, and their corresponding FE simulation setups. Section V presents results of the prototypical cubically symmetric lattices as test cases to validate the methods. Section VI presents results of effective stiffness tensors of the tetragonally symmetric and transversely isotropic test lattices, and we compare them in terms of their universal anisotropy index. In Sec. VII, we evaluate effective stiffness tensors of composite structures using the Bloch-wave homogenization method.

II. DESCRIPTION OF LATTICE GEOMETRIES

The unit cells of lattice geometries studied are shown in Fig. 1. The parent material of the lattices is modeled as polycarbonate with $E = 1$ GPa, $\nu = 0.35$, $\rho = 1097\,\mathrm{kg/m^3}$, and is considered isotropic. The lattice constant, L, is 8, 7, and 4 mm for foam, bowtie, and all other remaining lattices, respectively, and is kept constant throughout the geometric parameterization. The geometric parameterization includes internal cell angle, α, for the bowtie lattice and truss thickness, t, for all other lattices [Figs. 1(d), 1(e)]. The internal cell angle is varied from 55° to 90° with an interval of 2.5°, and truss thickness is varied from 0.1 to 1 mm at an interval of 0.1 mm. The internal cell angle of the bowtie lattice is studied in order to evaluate the lattice properties that span a negative to positive Poisson's ratio. As truss thickness increases the relative density of lattices also increases, whereas increase in the internal cell angle results in a decrease in relative density of the bowtie lattice. From the unit cell geometry of the bowtie lattice [Fig. 1(b)], it can be seen that it has 45° symmetry only in the XY plane, making it a tetragonal structure. We design another tetragonal unit cell by modifying the cubically symmetric octet lattice in such a way that it will have 45° symmetry only in the XY plane. To do so, we remove four internal

horizontal trusses [Fig. 1(c)], and we refer to this unit cell as the "octet-A" lattice. The hexagonal unit cell has infinite number of elastic symmetries in the XY plane, thus it is transversely isotropic with Z-direction being the out-of-plane axis. These unit cells are repeated spatially in 3D space to form an infinite array of lattice materials.

III. ELASTOSTATIC HOMOGENIZATION

We first calculate the effective properties of the lattice materials using appropriate static boundary conditions within a finite element method framework. To do this, we analyze a single unit cell and apply both periodic boundary conditions on all unit cell boundaries and classical boundary conditions of uniform displacement along the direction of interest. The apparent properties of the unit cell obtained under classical boundary conditions (displacement, traction or mixed) represent effective properties when the periodicity of the structure is incorporated.[13,27] We define the periodic boundary condition as

$$u_i^{+\hat{n}} - u_i^{-\hat{n}} = \epsilon_{ij}(x_j^{+\hat{n}} - x_j^{-\hat{n}}), \tag{1}$$

where u is the average displacement of the faces defined by unit normal vector, $\hat{n}$. Positive and negative signs indicate that the normal vectors representing a pair of periodic faces are opposite to each other, one being a source and other being a destination of the periodicity. ϵ and x are the macroscopic strain and nodal coordinates, respectively, in given i and j directions. For the abovementioned elastostatics boundary value problem, the constitutive equation for small strain deformation is $\sigma_{ij} = C_{ijkl}\epsilon_{kl}$, where σ and ϵ are the macroscopic stress and strain tensor, respectively, C is a fourth order stiffness tensor, and indices i, j, k, l take on values 1, 2, or 3. Our aim is to solve for this stiffness tensor and thereby evaluate the effective properties.

To evaluate the stiffness tensor constants of an effective continuum associated with uniaxial loading, we apply uniaxial displacement on opposing faces and then evaluate macroscopic stresses as

$$\sigma^* = \frac{\int_{A^*} dR}{\int_{A^*} dA^*}, \tag{2}$$

where σ^* is the effective stress acting on the effective surface area, A^*, on which the displacement, u, is applied, and R is the reaction force on that surface.[13] Effective strain, ϵ^*, is evaluated as the ratio of applied displacement, u, to the original length in that direction. We then use these macroscopic (or effective) stress-strain values in the constitutive equation (stiffness tensor, C, is now reduced to three non-zero independent constants due to uniaxial loading and periodic BCs) to evaluate the corresponding stiffness tensor constant. For example, when the displacement is applied along the X-direction with 3D periodicity then the stiffness tensor constants C_{11}^*, C_{12}^*, and C_{13}^* are evaluated. We replicate this same procedure in the other two directions, independently, to evaluate remaining stiffness tensor constants (C_{22}^*, C_{23}^*, and C_{33}^*). We then simulate pure shear loading (displacement based) in all planes, independently, to evaluate the stiffness tensor constants corresponding to shear moduli (C_{44}^*, C_{55}^*, and C_{66}^*). To simulate pure shear, we apply equal and opposite displacement on a pair of two opposite faces of the unit cell with planar boundary conditions on the third pair. We evaluate corresponding effective shear stress using Eq. (2) and effective shear strain based on the angle of deformation.

We performed elastostatic homogenization using commercial COMSOL MULTIPHYSICS (4.3b) software with standard physics controlled fine mesh. We used symmetric meshing on periodic faces for computational efficiency. We applied continuity periodic boundary conditions in three directions to simulate geometric periodicity of the lattices. The displacement and planar boundary conditions were applied using prescribed displacement. For cubic symmetry lattices, two static simulations were needed to obtain the stiffness tensor with three independent constants, whereas for transverse isotropy and tetragonal symmetric lattice, four static simulations, two with uniaxial loadings and two with shear loading, were required to obtain six and five independent stiffness tensor constants, respectively. We use these results as the reference for comparison with results from Bloch-wave homogenization method.

IV. BLOCH-WAVE HOMOGENIZATION

In this section, we apply the Bloch theorem to the elastostatics, where the structure of interest is periodic in nature, and its unit cell, when tessellated, will form an infinitely periodic structure. Bloch generalized Floquet's 1D mathematical result on to a 3D system to obtain the wave function that relates a simple plane wave with the periodicity of the structure.[28] We apply this concept to analyze the unit cell of an infinite lattice that eventually tells us the behavior of the entire structure.

We consider a lattice structure with two points, P and Q, with position vectors, $\vec{r}_P$ and $\vec{r}_Q$, respectively, at a distance from each other such that

$$\vec{r}_Q = \vec{r}_P + \vec{r}. \tag{3}$$

Here, we write position vector, $\vec{r}$, in terms of the lattice constant as $\vec{r} = n_i\hat{e}_i$, where n_i is unit cell number in the direction of unit vectors, $\hat{e}_i$. Assuming plane wave propagation, Bloch's theorem relates the displacement of any other point, Q, in any cell as

$$\vec{u}_Q(\vec{r}_Q, t) = \vec{u}_P e^{-i\left[\vec{k}(\vec{r}_Q - \vec{r}_P)\right]}, \tag{4}$$

where $\vec{k}$ is a wave vector. Since $\vec{r}_Q - \vec{r}_P$ is simply a function of the periodicity constant, we can identify the displacement of any other point within the lattice structure based on the analysis of a single unit cell for a known wave vector. We assume $\vec{k}$ is real, i.e., we neglect the attenuation in this analysis. One can further reduce the computational problem by restricting wave vectors to the edges of the irreducible Brillouin zone (IBZ)[29] for band gap analysis of periodic

structures.[2] However, in this paper, we analyze the long-wavelength wave propagation only along certain directions that we decide based on the number of independent stiffness tensor constants governed by the symmetry of the unit cell geometry. We then use the equations of motion to solve the eigenvalue problem of the propagating wave for the frequency, ω, at each combination of wave vectors. We obtain the dispersion curves (ω-k space) in the long wavelength limit, where the phase and group velocities are equal (denoted "V" hereafter) and are independent of frequency. We use this wave velocity information to analyze the lattice structures.

We determine the stiffness tensor constants, C^*_{ijkl}, of an effective continuum from the obtained wave velocities, V, through the Christoffel's equation[30]

$$\Gamma_{ik} = C^*_{ijkl} n_j n_l, \tag{5}$$

$$(\Gamma_{ik} - \delta_{ik}\rho^* V^2) P_m = 0, \tag{6}$$

where Γ is the acoustic tensor, ρ^* is the effective density, n_i is the direction cosine, P_m is the component of the unit vector in the displacement direction, and δ_{ik} is the Kronecker delta function. As each stiffness tensor constant is related to a particular type of propagating wave, identifying the wave polarization is essential (i.e., n_i and P_m must be known). In an effective elastic continuum, there exist three propagating waves within any structure: one longitudinal and two transverse. Generally, longitudinal velocities are higher than the transverse for an isotropic structure[2] and are independent of propagation direction. This is not always the case and it is non-trivial to identify the wave polarization within anisotropic structures. We also observe the existence of "quasi" waves when the wave propagates along any direction other than the principal axes in an anisotropic plane, and that the particle displacement is neither parallel nor perpendicular to the wave propagation direction.[31] Thus, we evaluate the propagating modal displacements to differentiate between the longitudinal and transverse waves. Further, for anisotropic structures, the two transverse velocities may not be equal, hence we use the wave propagation characteristics corresponding to a crystal symmetry in conjunction with the modal displacements and dispersion curves to identify the wave polarization.

This Bloch-wave homogenization method for effective material property evaluation is summarized in Fig. 2. We developed our wave propagation model within COMSOL MULTIPHYSICS (4.3b) using Floquet-Bloch periodic boundary conditions. We used physics controlled symmetric fine meshing for all our simulations with a very small range of wave vector [<1% of the lattice constant (1/m)] to ensure the applicability of effective continuum theory in long wavelength limit. We extracted the first three modes that correspond to the lowest longitudinal and two transverse waves of the lattice structure and calculated a best fit using least-squares regression to extract the wave velocities. We used volume averaged modal displacement along principal directions to identify the mode shapes and wave polarization.

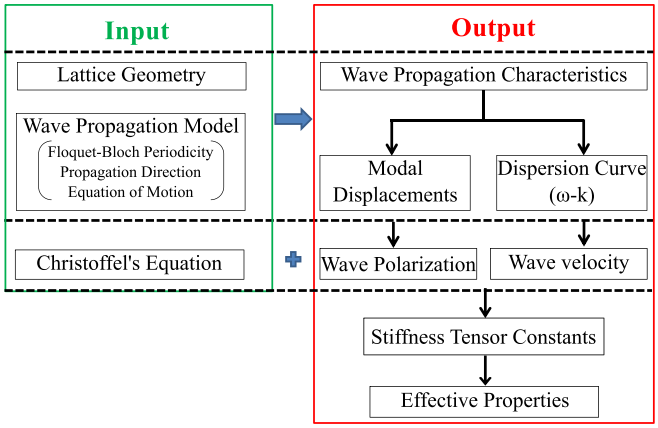

FIG. 2. (Color online) Schematic of Bloch-wave homogenization method.

V. EFFECTIVE PROPERTIES OF CUBIC SYMMETRY LATTICES

In this section, we present the Bloch-wave homogenization results of cubic symmetry lattices, using the octet lattice as an example case. By virtue of its geometry, the octet lattice has cubic symmetry and therefore three independent effective stiffness tensor constants: C_{11}, C_{12}, and C_{66}. The asterisk sign, which represents effective property has been dropped hereafter for convenience. These constants are related to corresponding wave velocities through the following reduced form of Christoffel's equation:

$$V_{xx} = \sqrt{C_{11}/\rho}, \tag{7}$$

$$V_{xy} = V_{xz} = \sqrt{C_{66}/\rho}, \tag{8}$$

$$2\rho V_{45}^2 = (C_{11} + C_{66}) \pm (C_{12} + C_{66}), \tag{9}$$

where for V_{ij}, i indicates the direction of wave propagation, and j indicates the direction of particle displacement. For V_ϕ, ϕ indicates the wave propagation angle with respect to principal axis. We evaluate the effective density,[1] ρ (asterisk dropped for convenience) based on the relative volume of the lattice and actual density of the parent bulk material. We use wave velocities along principal directions, i.e., longitudinal and transverse velocities, to identify the stiffness tensor diagonal elements, C_{11} and C_{66}, using Eqs. (7) and (8), respectively. The off-diagonal stiffness tensor constant can be calculated from waves propagating within any plane within the range of $0° < \phi < 90°$.[30] For simplicity of algebraic calculation, we select wave propagation at 45° in the XY plane (or 1–2 plane). We evaluate the off-diagonal constant using Eq. (9) based on either longitudinal or in-plane transverse velocity, where the sign is selected according to the type of polarization: positive for longitudinal wave and negative for in-plane transverse wave.[30]

The wave velocities and stiffness tensor constants of the octet lattice derived from Bloch-wave homogenization are shown in Fig. 3 with respect to relative density (lattice density normalized by bulk density). The evaluated stiffness tensor constants agree well with the static homogenization results. From the wave velocity results, one can observe that the transverse velocities are identical ($V_{xy} = V_{xz}$) when waves

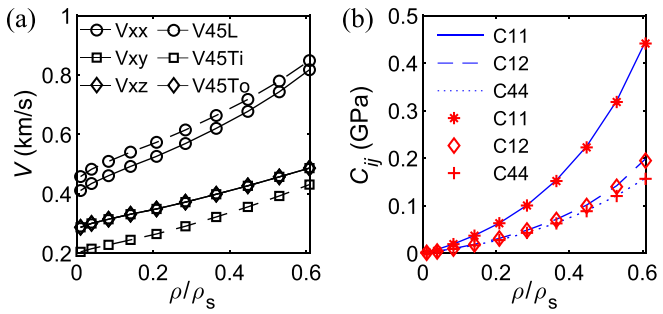

FIG. 3. (Color online) Octet lattice (a) wave velocities (note: $V_{xy}=V_{xz}=V_{45To}$) and (b) independent stiffness tensor constants evaluated from static (red markers) and Bloch-wave (blue lines) homogenization method.

propagate along the principal direction but different ($V_{45Ti} \neq V_{45To}$, where *Ti* and *To* stands for in-plane and out-of-plane transverse polarization, respectively) when waves propagate at an angle to the principal axes. This information is also useful in identifying the lattice symmetry. The relation between the in-plane transverse wave velocities along different directions ($V_{xy} > V_{45Ti}$) indicates that the octet lattice is stronger in shear along the principal direction. On the other hand, the relation between the longitudinal wave velocities along different directions ($V_{45L} > V_{xx}$, where *L* indicates longitudinal polarization) indicates that the octet lattice is stronger in compression along the 45° axis.

We apply Bloch-wave homogenization to the cubic, foam, and Kelvin lattices, and their effective properties along with octet lattice are shown normalized with respect to properties of the bulk material (Fig. 4). Results of the Kelvin lattices are presented only up to truss thickness of 0.8 mm since the geometry changes at higher values. We show the relationship between the logarithm of the relative modulus and relative density of these lattices for low relative densities in Figs. 4(d), 4(e). We then calculate the polynomial best fit of initial five data points through least-squares regression and obtain the power law relationship between the actual quantities as $E/E_s \propto (\rho/\rho_s)^m$ and $G/G_s \propto (\rho/\rho_s)^n$. The exponents, *m* and *n*, of the power laws correspond to the slopes of the lines in log plots. An exponent of *m*, $n=1$ signifies that the geometry is stretch-dominant, while an exponent of *m*, $n=2$ indicates that the geometry is bending-dominant.[32] We see that for the lower values of relative densities, $E/E_s \propto \rho/\rho_s$ and $G/G_s \propto \rho/\rho_s$ for the octet lattice as also shown theoretically by Deshpande *et al.*,[8] whereas for the Kelvin lattice, $E/E_s \propto (\rho/\rho_s)^2$ and $G/G_s \propto (\rho/\rho_s)^2$ as shown experimentally by Zheng *et al.*[25] The foam lattice effective properties also scales with $(\rho/\rho_s)^2$, whereas cubic lattice shows combined behavior with $E/E_s \propto \rho/\rho_s$ under uniaxial compression but $G/G_s \propto (\rho/\rho_s)^2$ under shear loading. Consistent with much prior work, at lower relative densities, the octet lattice is stretch dominant,[25,32] the foam and Kelvin lattices are bending dominant,[25] and the cubic lattice is stretch dominant in compression but bending dominant in shear. As the relative density increases, the linear relation between relative modulus and relative density of the octet lattice becomes non-linear [Fig. 4(a), 4(b)] signifying the truss bending effect during deformation. Overall, the Kelvin lattice is much weaker in uniaxial loading compared to cubic lattice as observed by Hedayati *et al.*[33] However, in contrast to their shear modulus predictions, we find that the Kelvin lattice has a higher shear modulus compared to the cubic lattice (truss beam modeling and rigid vertices are possibly making the cubic lattice more shear resistant in Hedayati

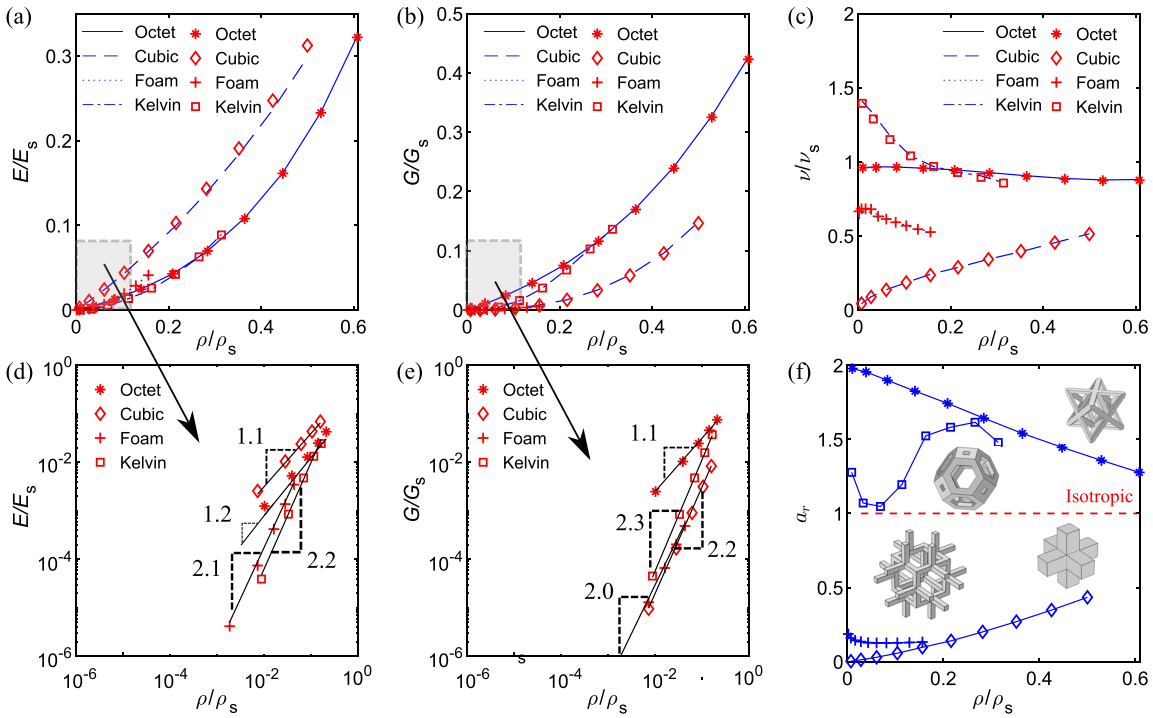

FIG. 4. (Color online) Normalized effective mechanical properties (a) uniaxial modulus, (b) shear modulus, and (c) Poisson's ratio of cubic symmetry lattices. Magnified logarithmic plots of shaded area of (a) and (b) are shown in (d) and (e) for better visualization of low relative density results with numerical values indicating slopes. (f) Zener anisotropy index of cubic symmetry lattices.

et al.[33]). The truss joints in the Kelvin geometry are thus stronger than in the foam and cubic geometry.

We also see that the octet lattice almost maintains a constant Poisson's ratio [Fig. 4(c)] at low relative densities and deviates slightly at higher relative densities. The absolute value of the octet lattice Poisson's ratio is also almost same as that of the parent bulk material, which indicates that the macroscopic deformation in octet lattice is analogous to bulk material deformation. For both cubic and foam lattices, there is a steep increase in Poisson's ratio initially, possibly due to negligible bending resistance contributing to lateral deformation. For the cubic lattice, the increase in lateral deformation is always higher than the uniaxial deformation (due to stretch dominant behavior) and thus Poisson's ratio increases throughout. Kelvin and foam lattice, due to their bend dominant characteristic, offers significant bending stiffness and thus as relative density increases, their Poisson's ratio decreases.

We compare these cubic symmetry lattices by evaluating their Zener anisotropy index,[34] $a_r = 2C_{44}/(C_{11} - C_{12})$, shown in Fig. 4(f). While the Zener anisotropy index is limited to cubic symmetry lattices, it gives important insights on the variation in Young's modulus with direction, which is not possible with other anisotropy indices such as the universal anisotropy index (UAI) discussed later in Sec. VI. All the lattices have non-unity anisotropy index, and as relative density increases they tend to become more isotropic. The cubic and foam lattices have an index less than unity, indicating their maximum Young's modulus is along the $\langle 100 \rangle$ direction and minimum along the $\langle 111 \rangle$ direction. For Kelvin and octet lattice, the case is reversed: the maximum Young's modulus is along the $\langle 111 \rangle$ direction and minimum along the $\langle 100 \rangle$ direction, as they have an index greater than unity. In other words, the cubic and foam lattices are stronger in compression along principal axes but weaker along the space diagonal (the opposite case is true for Kelvin and octet), as shown through normalized Young's modulus representational surface (of cubic and Kelvin) by Luxner *et al.*[24] It should be noted that the anisotropy index of the octet lattice shown here is consistent with Berger *et al.*,[35] where they have evaluated reciprocal of Zener anisotropy index.

VI. EFFECTIVE PROPERTIES OF LOWER SYMMETRY LATTICES

Here, we apply the Bloch-wave homogenization to evaluate effective properties of higher anisotropy structures. We consider the tetragonal and transversely isotropic symmetry structures, which have six and five independent stiffness tensor constants, respectively.

A. Tetragonal symmetry lattices

We analyze two tetragonal symmetry lattices: a new form of octet lattice, termed "octet-A," as discussed in Sec. II [refer Fig. 1(c)], and a bowtie lattice of tetragonal symmetry that can behave auxetically (negative Poisson's ratio) by virtue of its re-entrant truss structure. The Poisson's ratios of these two lattices obtained from static simulations are shown in Fig. 5. The octet-A lattice has positive Poisson's ratio in all planes whereas the bowtie lattice has negative Poisson's ratio that changes to positive as the internal cell angle, α [Fig. 1(e)] increases. There are also instances ($87.5° \geq \alpha \geq 80°$) for the bowtie lattice, where Poisson's ratio is negative in two planes (XZ and YZ) but positive in the other (XY). At $\alpha = 90°$, the bowtie lattice has positive Poisson's ratio throughout and thus loses its auxetic behavior. At 88° the Poisson's ratio in the XZ plane is independent of the loading direction as $\nu_{xz} = \nu_{zx}$.

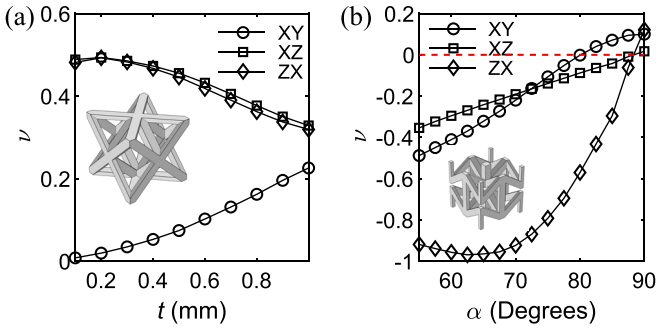

FIG. 5. (Color online) Poisson's ratio of (a) octet-A and (b) bowtie lattice. Dashed red line is zero reference line.

To calculate the effective stiffness tensor diagonal elements, we first calculate the wave velocities along the principal directions. To distinguish between longitudinal and transverse waves, we exploit the symmetries of the tetragonal structure, where one of the transverse X-direction waves has the same velocity as that of the transverse Z-direction wave. Once the principal wave velocities are known, we use Christoffel's equation to evaluate the diagonal stiffness tensor constants. The diagonal constants C_{11}, C_{33}, C_{44}, and C_{66} are directly related to the following wave velocities through the reduced form of Christoffel's equation:

$$V_{xx} = \sqrt{C_{11}/\rho}, \tag{10a}$$

$$V_{zz} = \sqrt{C_{33}/\rho}, \tag{10b}$$

$$V_{xy} = \sqrt{C_{66}/\rho}, \tag{10c}$$

$$V_{zx} = \sqrt{C_{44}/\rho}. \tag{10d}$$

Note that $V_{xx} = V_{yy}$, $V_{xy} = V_{yx}$, and $V_{zx} = V_{xz} = V_{zy} = V_{yz}$ by virtue of the tetragonal symmetry. The obtained wave velocities and corresponding stiffness tensor constants are shown in Figs. 6(a), 6(b) and Figs. 6(c)–6(f), respectively. We see that the diagonal stiffness tensor constants calculated from Bloch-wave homogenization agree with that of static homogenization method for both the lattices.

To evaluate the off-diagonal stiffness tensor constants, we calculate velocities of waves propagating at 45° to the principal axes. The angle 45° is again selected to mathematically simplify the expressions, but any other angle ($0° < \phi < 90°$) would work.[30,36] For waves propagating in the XY plane, there exist pure waves as properties are symmetric about 45° axes. In the case of anisotropic plane XZ, we observe one quasi-longitudinal (QL) and two quasi-transverse (QT) waves. To identify the polarization of waves propagating at an angle to the principal axis, we use

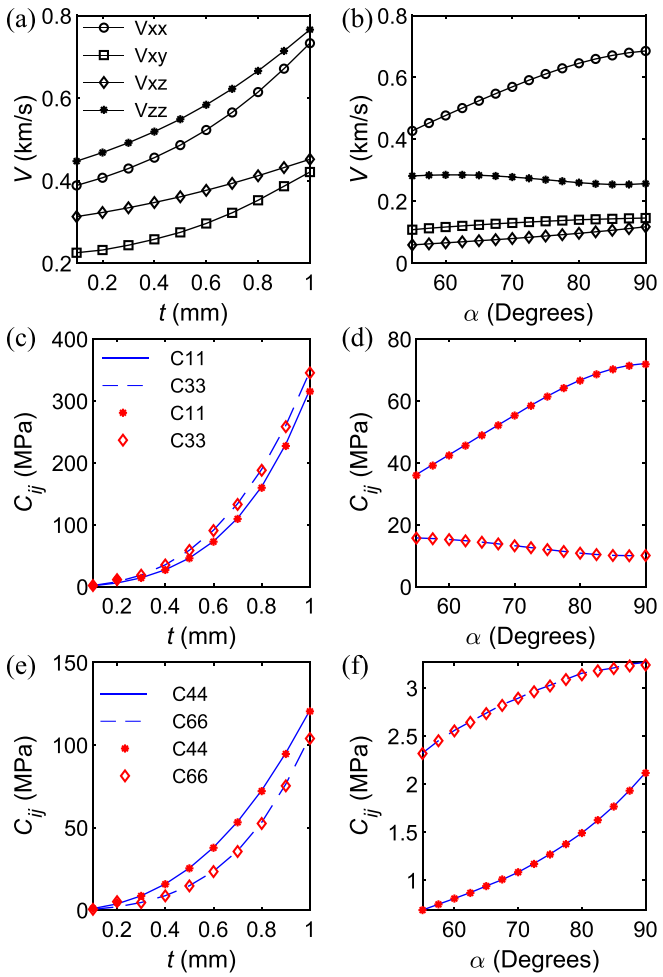

FIG. 6. (Color online) Principal direction wave velocities of (a) octet-A and (b) bowtie lattice. Evaluated diagonal stiffness tensor constants from static (red markers) and Bloch-wave (blue lines) homogenization of octet-A [(c) and (e)] and bowtie [(d) and (f)] lattices. Bowtie lattice plots follow the same legend scheme as that of octet-A plots.

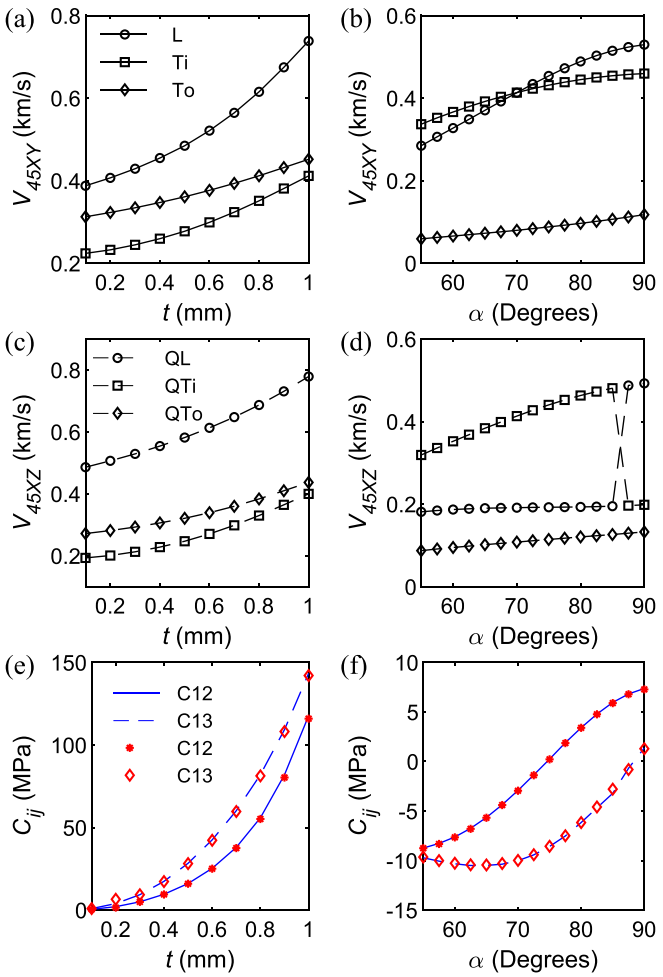

FIG. 7. (Color online) Non-principal directional wave velocities of octet-A lattice in (a) XY plane and (c) XZ plane; and of bowtie lattice in (b) XY plane and (d) XZ plane. L, Ti, To, and Q stand for longitudinal, in-plane transverse, out-of-plane transverse, and quasi waves, respectively. Resulting off-diagonal stiffness tensor constants of (e) octet-A and (f) bowtie lattice evaluated from static (red markers) and Bloch-wave (blue lines) homogenization. Bowtie lattice plots follow the same legend scheme as that of octet-A plots.

global modal displacement corresponding to each mode shape. We differentiate between longitudinal, in-plane transverse, and out-of-plane transverse waves based on the dominant modal displacement corresponding to each mode. The calculated wave velocities at 45° in XY (V_{45XY}) and XZ (V_{45XZ}) planes are shown in Figs. 7(a)–7(d).

The generalized form of Christoffel's equation to evaluate C_{12} of an orthotropic structure[30] for wave propagation at any angle, ϕ, in XY plane is given as

$$C_{12} = -C_{66} \pm \sqrt{\frac{2\rho V_{\phi XY}^2 - \chi_1 - \Gamma_1^2}{4n_1^2 n_2^2}}, \tag{11}$$

where $\chi_1 = C_{11}n_1^2 + C_{66}n_2^2 + C_{22}n_2^2 + C_{66}n_1^2$ and $\Gamma_1 = C_{11}n_1^2 + C_{66}n_2^2 - C_{22}n_2^2 - C_{66}n_1^2$. The wave direction vectors are defined as $n_1 = \cos\phi$ and $n_2 = \sin\phi$. The term $V_{\phi ij}$ indicates the waves (1 longitudinal, 1 in-plane transverse and 1 out-of-plane transverse) propagating in i-j plane at ϕ° to i-axis. It is important to note that either the longitudinal or in-plane transverse wave velocity can be used to identify the corresponding stiffness tensor constants;[30] the sign in front of the square root depends on the type of wave velocity used. For the case of C_{12}, the sign of the square root is positive when using the longitudinal wave and negative when using the transverse wave; both lead to the same solution of C_{12}. Since the tetragonal structures have same properties along X and Y direction, we further simplify Eq. (11) for $\phi = 45^\circ$ as

$$C_{12} = 2\rho V_{45XYL}^2 - C_{11} - 2C_{66}, \tag{12a}$$

$$C_{12} = -2\rho V_{45XYTi}^2 + C_{11}. \tag{12b}$$

The generalized form of Christoffel's equation to evaluate C_{13} of an orthotropic structure for wave propagation at angle ϕ in the XZ plane is given as

$$C_{13} = -C_{44} \pm \sqrt{\frac{2\rho V_{\phi XZ}^2 - \chi_2 - \Gamma_2^2}{4n_1^2 n_3^2}}, \tag{13}$$

where $\chi_2 = C_{11}n_1^2 + C_{44}n_3^2 + C_{33}n_3^2 + C_{44}n_1^2$ and $\Gamma_2 = C_{11}n_1^2 + C_{44}n_3^2 - C_{33}n_3^2 - C_{44}n_1^2$. The wave direction vectors are defined as $n_1 = \cos\phi$ and $n_3 = \sin\phi$. In the case of C_{13}, we determine the sign of the square root purely based on the

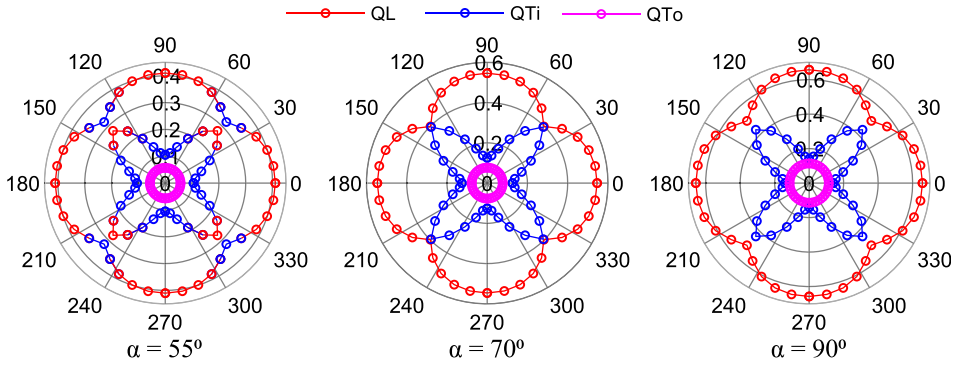

FIG. 8. (Color online) Iso-frequency contour of bowtie lattice wave velocities in XY plane, showing change in faster wave polarization around $\phi = 45°$ for $\alpha = 55°$. Theta in polar plot is wave propagation angle, ϕ (in degrees), in XY plane and radius is the wave velocity, V (in km/s).

sign of XZ plane Poisson's ratio (ν_{zx}) of the structure, and either of the QL or in-plane QT velocities can be used. When the lattice has a negative Poisson's ratio, the off-diagonal stiffness tensor constant must be negative, and vice versa. So, we use a positive root for octet-A lattice but for bowtie, we use a negative sign up to $\alpha < 87.5°$. For the last two angles studied, the Poisson's ratio is either zero or positive, and taking positive root is essential. The calculated off-diagonal stiffness tensor constants are shown in Figs. 7(e), 7(f). For both the octet-A and bowtie lattices, the results agree with static homogenization results. For the bowtie lattice, the off-diagonal stiffness tensor constants change signs from negative to positive signifying the change in the sign of Poisson's ratio.

The bowtie lattice exhibits an unusual wave polarization transition. Specifically, we observe a shift in faster wave polarization in both planes for the bowtie lattice [Figs. 7(b) and 7(d)]. For smaller values of α, transverse velocity is higher, whereas for larger angles, the longitudinal velocity is higher. This shift occurs at $\alpha = 70°$ for V_{45XY}, and at $\alpha = 86.25°$ for V_{45XZ}. To illustrate this polarization shift, we show the wave velocity field of the bowtie lattice in the XY plane through an iso-frequency contour (Fig. 8). For the bowtie lattice geometry at $\alpha = 55°$, the in-plane transverse wave has a higher velocity than the longitudinal wave around 45° propagation direction. However, for $\alpha = 90$, the longitudinal wave propagates faster than the transverse wave at all propagation angles. This wave polarization transition is not present in the octet-A lattice within the parameters studied: the longitudinal wave always remains faster than the transverse waves [Figs. 7(a) and 7(c)].

This anomalous behavior has been discussed by Helbig and Schoenberg[37] in a transversely isotropic structure through the analysis of slowness surfaces. In general, for anisotropic materials with $\nu > 0$, the longitudinal wave propagates with a faster velocity because $C_{12} + C_{66} > 0$ and $C_{13} + C_{44} > 0$.[37,38] If C_{12} or C_{13} are negative (a case of auxetic structure) and greater than C_{66} and C_{44}, respectively, then the respective transverse wave is faster than the longitudinal wave. In our bowtie lattice, $C_{12} + C_{66} < 0$ when $\alpha < 70°$ and $C_{13} + C_{44} < 0$ when $\alpha < 86.25°$, thus the respective transverse waves travel faster at angles less than these values, which our results clearly show [Fig. 6(f) and Figs. 7(b) and 7(d), 7(f)]. The transverse and longitudinal wave velocities are equal at the acoustic axes or singularities,[39] when $C_{12} = -C_{66}$ ($\alpha = 70°$) and $C_{13} = -C_{44}$ ($\alpha = 86.25°$). This anomalous polarization behavior has been observed in few natural materials such as calcium formate,[40] and can be utilized in potential metamaterials applications such as mode conversion.[40]

B. Transversely isotropic symmetry lattice

The lattices discussed thus far have periodicity in three orthogonal directions. In this section, we evaluate effective properties of a hexagonal lattice that has periodicity in three directions: e_1, e_2, and e_3, of which one pair is not mutually perpendicular, e_1 and e_2, as shown in Fig. 9(a). This hexagonal lattice has five independent stiffness tensor constants. We obtain identical wave propagation results in the XY plane irrespective of the direction of wave propagation, since the hexagonal lattice has one isotropic plane (XY in this case). The obtained effective properties are shown in Fig. 9(b). The stiffness tensor constant C_{12} calculated from the wave velocities, V_{45XY}, using Eq. (12a) or (12b) matches with the one calculated using characteristics of transversely isotropic structure, i.e., based on C_{11} and C_{66} ($C_{12} = C_{11} - 2C_{66}$).

C. Anisotropy index of lower symmetry lattices

In order to compare the lower symmetry lattices discussed in this section as well as the cubic lattices discussed in Sec. V, we evaluate Universal Anisotropy Index (UAI)[41] that quantifies the extent of anisotropy of any symmetry material. The UAI is defined as

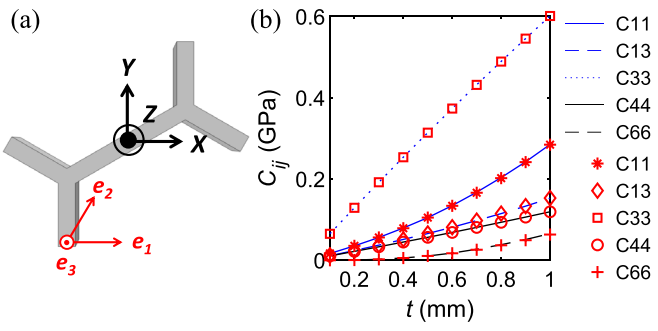

FIG. 9. (Color online) (a) Hexagonal unit cell with periodicity direction vectors and (b) effective stiffness tensor constants evaluated through static (red markers) and Bloch-wave (blue lines) homogenization method.

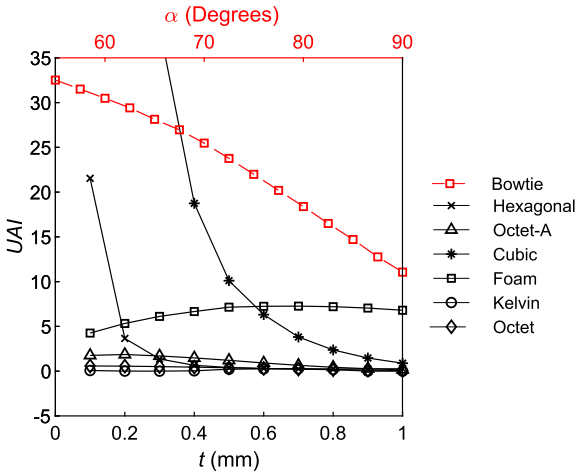

FIG. 10. (Color online) Universal anisotropy index of 3D lattices. Cubic lattice UAI values for truss thickness 0.1, 0.2, and 0.3 mm are 426, 95, and 38, respectively.

$$A^U = 5\frac{G^V}{G^R} + \frac{K^V}{K^R} - 6. \tag{14}$$

Here, superscript V corresponds to Voigt estimates and R corresponds to Reuss estimates of bulk, K, and shear, G, modulus. Specifically,

$$G^V = \frac{1}{15}\left(C_{ijij} - \frac{1}{3}C_{iijj}\right), \tag{15a}$$

$$\frac{1}{G^R} = \frac{2}{5}\left(S_{ijij} - \frac{1}{3}S_{iijj}\right), \tag{15b}$$

$$K^V = \frac{1}{9}C_{iijj}, \tag{15c}$$

$$\frac{1}{K^R} = S_{iijj}, \tag{15d}$$

which we calculate from the effective stiffness tensor, C, and compliance tensor, S, where $S = C^{-1}$.

The dependence of UAI on geometric parameters for all lattices is shown in Fig. 10. The bowtie lattice has a higher anisotropy than both octet-A and hexagonal, whereas hexagonal is much closer to the UAI value of 0 (zero UAI indicates isotropic behavior as opposed to unity for Zener anisotropy index) indicating more isotropic behavior than others. There is a sudden shift in the extent of anisotropy for hexagonal lattice (also for cubic lattice) as truss thickness increases from very small thicknesses. This is due to the fact that at very low truss thickness the bending resistance from lattice trusses is negligible, which becomes more prominent as thickness increases.

VII. EFFECTIVE PROPERTIES OF COMPOSITE STRUCTURES

As a final demonstration of the Bloch-wave homogenization method, we design 3D periodic composite structures with lattice reinforcements and evaluate their effective properties. We design these composite structures by filling the volume surrounding to the lattice (within the unit cell) with a second material. These composite structures enable us to obtain properties that are a mixture of two bulk materials and the lattice geometry. They are potential multifunctional metamaterials, as such structures have already shown enhanced macroscopic strength and energy absorption properties.[42] Such composite structures can be readily fabricated by commercial multi-material 3D printers. Once the lattice geometry is modeled, we form the complementary part of this lattice within the unit cell using Boolean operations and then combine these two designs to form a composite structure (Fig. 11). We assume a complete bonded contact (no slip) between the lattice and filler material surface. This ensures the displacement continuity at the interface and satisfies mechanical compatibility during quasi-static and Bloch-wave analysis.

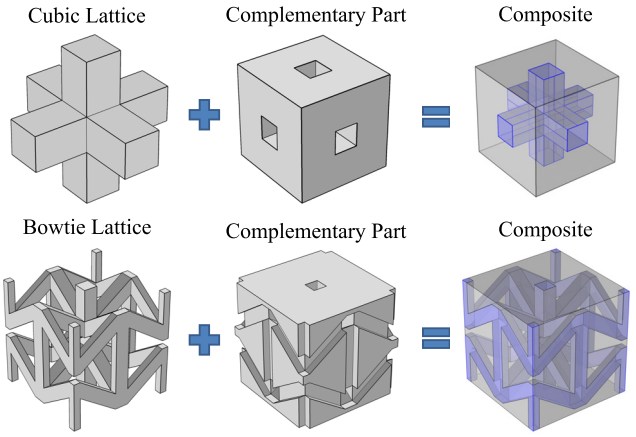

FIG. 11. (Color online) Composite structure solid modeling (complementary part is designed by subtracting lattice geometry from bulk unit cell volume).

Here, we study composites formed from cubic, octet, and bowtie lattices. We manipulate the properties and anisotropy of these composites by changing the modulus of the filler material. We keep the same lattice bulk material properties as before, and consider three cases of the filler material with moduli ratio (MR: ratio of filler bulk Young's modulus to lattice bulk Young's modulus): 50% ($E_{filler} = 0.5$ GPa), 5% ($E_{filler} = 0.05$ GPa), and 0.5% ($E_{filler} = 0.005$ GPa). To isolate the effect of modulus change, we model the density and Poisson's ratio of the filler material the same as that of the lattice bulk material.

A. Effective properties of bowtie composite structures

As an example, we present the effective properties of the bowtie composite, with filler moduli ratio of 0.5% [Fig. 12(a)] evaluated through Bloch-wave homogenization. This bowtie composite structure is auxetic up until internal cell angle, $\alpha_{aux} = 80°$ [Fig. 12(a)] as opposed to pure bowtie lattice where $\alpha_{aux} \approx 87.5°$ [Fig. 7(f)]. For the higher moduli ratios (5% and 50%), the bowtie composite is no longer auxetic (within studied range of internal cell angles), as the filler material counteracts the deformation pattern of the re-entrant trusses (results not shown). In the case of 0.5% MR, the change in faster wave polarization is not observed even though the composite structure is auxetic, since the magnitude of the diagonal stiffness tensor constants corresponding to shear are always higher than the off-diagonal negative

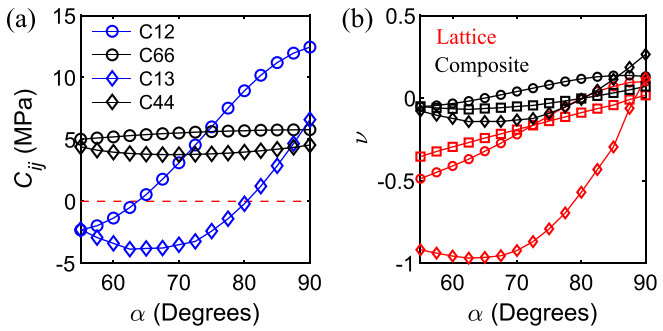

FIG. 12. (Color online) Effective stiffness tensor constants of the bowtie composite structure with 0.5% moduli ratio: (a) C_{12}, C_{66}, C_{13}, C_{44} (dashed red line is a zero-reference line), and (b) Poisson's ratio of bowtie lattice (red) compared to bowtie composite structure (black) (ν_{xy}, ν_{xz}, ν_{zx} are shown in circle, square, and diamond markers, respectively).

stiffness tensor constants [Fig. 12(a)]. The change in the sign of Poisson's ratio is also observed at a different lattice geometry [Fig. 12(b)]: in the XY plane, $\alpha_{aux} \approx 65°$ ($\alpha_{aux} = 80°$ in the pure lattice), whereas in the XZ plane $\alpha_{aux} \approx 80°$ ($\alpha_{aux} \approx 87.5°$ in the pure lattice). The overall stiffness of the composite structure is also higher than the pure bowtie lattice stiffness [Figs. 12(a) and Fig. 6(f)]. These results show that in addition to changing the geometric parameters, changing the modulus of filler materials in composite structures can tune the overall macroscopic elastic performance of the structure.

B. Anisotropy index of composite structures

The cubic and octet composite structures are cubic in symmetry since both lattice and filler are cubically symmetric. To observe the effect of filler material on pure lattices, we evaluate Zener anisotropy index [Fig. 13(a)] for moduli ratio of 5% and 50%. We observe that both cubic and octet composite structures with 50% moduli ratio are nearly isotropic, specifically at lower truss thicknesses. This is because the contribution of cubic and octet lattices in the overall structural properties is comparatively negligible. As lattice truss thickness increases, the composite structure deviates slightly from this isotropic behavior. When the moduli ratio is 5%, the lattice plays a more prominent role in the overall strength; the anisotropy of the composite structure is dominated by the lattice. The maximum anisotropy of these composites occurs at truss thickness, t, of 0.7 mm as opposed to 0.1 mm for the pure lattices.

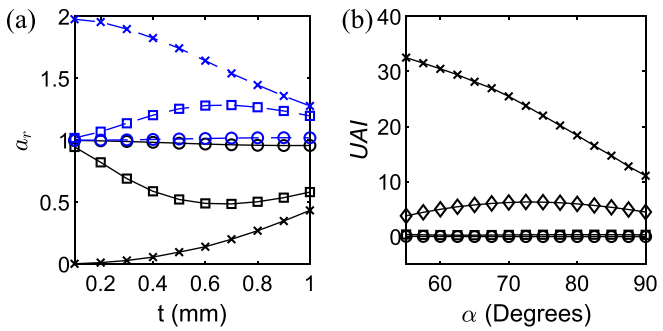

FIG. 13. (Color online) (a) Zener anisotropy index of cubic symmetry lattices and composites. Cubic and octet results are shown in black solid and blue dashed linestyle, respectively, and lattice, 5% and 50% MR composites are shown in cross, square, and circle markers, respectively. (b) Universal anisotropy index of bowtie lattice and composites. Lattice, 0.5%, 5%, and 50% MR composites are shown in cross, diamond, square, and circle markers, respectively. 5% and 50% MR composites UAI values are overlapping and close to zero.

We compare the elastic behavior of the bowtie composites with the pure lattice based on UAI evaluated through Eq. (14). For 50% and 5% moduli ratio, the composite behaves almost isotropically [UAI = 0, Fig. 13(b)]. Again, here the stiffness is dominated by the filler material rather than the lattice. For much softer filler material (0.5% moduli ratio), the bowtie lattice maintains some anisotropy. These results show that we can decrease the anisotropy of the composite structure by increasing the modulus of the filler material.

VIII. CONCLUSION

In this article, we reviewed the displacement-based elastostatic and Bloch-wave homogenization methods within a finite element method framework for effective property evaluation of 3D periodic lattices. We applied these methods to evaluate effective elastic properties of anisotropic lattices with cubic, tetragonal, and transversely isotropic symmetry, including an auxetic geometry. Results obtained from Bloch-wave homogenization agree well with static homogenization results for different symmetries, relative densities, truss orientations, and non-principal periodicities. We compared various lattices based on their anisotropic behavior through Zener and Universal anisotropy index. We extended this approach to analyze composite structures with lattice reinforcements, and our results show that the anisotropy and elastic performance of these structures can be manipulated without modifying the lattice geometry, but instead by modifying relative bulk material properties of the lattice and surrounding material.

The Bloch-wave homogenization approach studied in this article will open new directions to study the effect of geometry and bulk material properties on the static as well as dynamic properties of the structure simultaneously, and can accelerate the process of analyzing periodic structures to achieve certain vibration characteristics such as band gaps, mode shapes, and energy propagation, in addition to their static effective properties. By changing the anisotropy of the structure, we show it is possible to control the wave propagation in a certain direction with or without minimal change in other directions. Future work in this process will include experimental verification of evaluated effective properties of lattices. This method can be extended to develop multifunctional structural materials, where tailored vibration mitigation, high impact absorption, and optimum static properties are required. The bridge between wave velocities and mechanical properties of lattice structures is also useful in nondestructive evaluation (NDE) of metamaterials through wave velocity measurements. This analysis lays the groundwork to explore NDE of lattice metamaterials in terms of quantifying mechanical property degradation through ultrasonic velocity measurements.

[1]L. J. Gibson and M. F. Ashby, *Cellular Solids: Structure and Properties*, Cambridge Solid State Science Series, 2nd ed. (Cambridge University Press, Cambridge, UK, 1997), pp. 1–217.
[2]A. S. Phani, J. Woodhouse, and N. A. Fleck, "Wave propagation in two-dimensional periodic lattices," J. Acoust. Soc. Am. **119**(4), 1995–2005 (2006).
[3]Y. Chen and L. Wang, "Harnessing structural hierarchy to design stiff and lightweight phononic crystals," Extreme Mech. Lett. **9**, 91–96 (2016).
[4]K. H. Matlack, A. Bauhofer, S. Krödel, A. Palermo, and C. Daraio, "Composite 3D-printed meta-structures for low frequency and broadband vibration absorption," Proc. Natl. Acad. Sci. U.S.A. **113**(30), 8386–8390 (2016).
[5]H. J. Rathbun, D. D. Radford, Z. Xue, M. Y. He, J. Yang, V. Deshpande, N. A. Fleck, J. W. Hutchinson, F. W. Zok, and A. G. Evans, "Performance of metallic honeycomb-core sandwich beams under shock loading," Int. J. Solids Struct. **43**(6), 1746–1763 (2006).
[6]T. A. Schaedler, A. J. Jacobsen, A. Torrents, A. E. Sorensen, J. Lian, J. R. Greer, L. Valdevit, W. B. Carter, Q. Ge, J. A. Jackson, S. O. Kucheyev, N. X. Fang, and C. M. Spadaccini, "Ultralight metallic microlattices," Science **334**(6058), 962–965 (2011).
[7]D. Mahmoud and M. Elbestawi, "Lattice structures and functionally graded materials applications in additive manufacturing of orthopedic implants: A review," J. Manufact. Mater. Process. **1**(2), 1–19 (2017).
[8]V. S. Deshpande, N. A. Fleck, and M. F. Ashby, "Effective properties of the octet-truss lattice material," J. Mech. Phys. Solids **49**(8), 1747–1769 (2001).
[9]D. H. Chen, "Bending deformation of honeycomb consisting of regular hexagonal cells," Compos. Struct. **93**(2), 736–746 (2011).
[10]J. Hohe and W. Becker, "A refined analysis of the effective elasticity tensor for general cellular sandwich cores," Int. J. Solids Struct. **38**(21), 3689–3717 (2001).
[11]F. Scarpa, P. Panayiotou, and G. Tomlinson, "Numerical and experimental uniaxial loading on in-plane auxetic honeycombs," J. Strain Anal. Eng. Des. **35**(5), 383–388 (2000).
[12]J. C. Wallach and L. J. Gibson, "Mechanical behavior of a three-dimensional truss material," Int. J. Solids Struct. **38**(40-41), 7181–7196 (2001).
[13]A. S. Dalaq, D. W. Abueidda, R. K. Abu Al-Rub, and I. M. Jasiuk, "Finite element prediction of effective elastic properties of interpenetrating phase composites with architectured 3D sheet reinforcements," Int. J. Solids Struct. **83**, 169–182 (2016).
[14]M. S. A. Elsayed and D. Pasini, "Analysis of the elastostatic specific stiffness of 2D stretching-dominated lattice materials," Mech. Mater. **42**(7), 709–725 (2010).
[15]M. S. A. Elsayed, "Multiscale mechanics and structural design of periodic cellular materials," Ph.D. dissertation, McGill University, Montreal, Canada, 2010.
[16]P. Chopra, "Effective mechanical properties of lattice materials," M.A. Sc. dissertation, University of British Columbia, Vancouver, Canada, 2011.
[17]Y. Lai, Y. Wu, P. Sheng, and Z. Q. Zhang, "Hybrid elastic solids," Nat. Mater. **10**(8), 620–624 (2011).
[18]S. Krödel, T. Delpero, A. Bergamini, P. Ermanni, and D. M. Kochmann, "3D auxetic microlattices with independently controllable acoustic band gaps and quasi-static elastic moduli," Adv. Eng. Mater. **16**(4), 357–363 (2014).
[19]A. S. Phani and Mahmoud I. Hussein, *Dynamics of Lattice Materials*, 1st ed. (Wiley, New York, 2017), pp. 19–87.
[20]M. C. Messner, M. I. Barham, M. Kumar, and N. R. Barton, "Wave propagation in equivalent continuums representing truss lattice materials," Int. J. Solids Struct. **73-74**, 55–66 (2015).
[21]Y. H. Lee and T. Oh, "The measurement of P-, S-, and R-wave velocities to evaluate the condition of reinforced and prestressed concrete slabs," Adv. Mater. Sci. Eng. **2016**, 1548215 (2016).
[22]U. B. Halabe, G. M. Bidigalu, H. V. S. Gangarao, R. J. Ross, E. Ecmpd, and E. E. Eswd, "Nondestructive evaluation of green wood using stress wave and transverse vibration techniques," Mater. Eval. **55**(9), 1013–1018 (1995).
[23]H. Ogi, M. L. Dunn, K. Takashima, and H. Ledbetter, "Elastic properties of a unidirectional SiCf/Ti composite: Acoustic-resonance measurements and micromechanics predictions," J. Appl. Phys. **87**(6), 2769–2774 (2000).
[24]M. H. Luxner, J. Stampfl, and H. E. Pettermann, "Numerical simulations of 3D open cell structures—Influence of structural irregularities on elasto-plasticity and deformation localization," Int. J. Solids Struct. **44**(9), 2990–3003 (2007).
[25]X. Zheng, H. Lee, T. H. Weisgraber, M. Shusteff, J. DeOtte, E. B. Duoss, J. D. Kuntz, M. M. Biener, Q. Ge, J. A. Jackson, S. O. Kucheyev, N. X. Fang, and C. M. Spadaccini, "Ultralight, ultrastiff mechanical metamaterials," Science **344**(6190), 1373–1377 (2014).
[26]H. M. Kolken and A. A. Zadpoor, "Auxetic mechanical metamaterials," RSC Adv. **7**(9), 5111–5129 (2017).
[27]M. Jiang, I. Jasiuk, and M. Ostoja-Starzewski, "Apparent elastic and elastoplastic behavior of periodic composites," Int. J. Solids Struct. **39**(1), 199–212 (2002).
[28]F. Bloch, "Über die Quantenmechanik der Elektronen in Kristallgittern," Z. Phys. A **52**(7-8), 555–600 (1929).
[29]C. Kittel, *Introduction to Solid State Physics*, 8th ed. (Wiley, New York, 2010), pp. 33–37.
[30]Voichita Bucur, *Acoustics of Woods*, Springer Series in Wood Science, 2nd ed. (Springer-Verlag, Berlin, Germany, 2006), pp. 49–55.
[31]A. Van Pamel, G. Sha, S. I. Rokhlin, and M. J. S. Lowe, "Finite-element modelling of elastic wave propagation and scattering within heterogeneous media," Proc. R. Soc. A: Math. Phys. Eng. Sci. **473**(2197), 20160738 (2016).
[32]N. A. Fleck, V. S. Deshpande, and M. F. Ashby, "Micro-architectured materials: Past, present and future," Proc. R. Soc. A: Math. Phys. Eng. Sci. **466**(2121), 2495–2516 (2010).
[33]R. Hedayati, M. Sadighi, M. Mohammadi-Aghdam, and H. Hosseini-Toudeshky, "Comparison of elastic properties of open-cell metallic biomaterials with different unit cell types," J. Biomed. Mater. Res. Part B: Appl. Biomater. **106**(1), 386–398 (2018).
[34]C. M. Zener and S. Siegel, "Elasticity and anelasticity of metals," J. Phys. Colloid Chem. **53**(9), 1468–1468 (1949).
[35]J. B. Berger, H. N. Wadley, and R. M. McMeeking, "Mechanical metamaterials at the theoretical limit of isotropic elastic stiffness," Nature **543**(7646), 533–537 (2017).
[36]B. C. Abell, S. Shao, and L. J. Pyrak-Nolte, "Measurements of elastic constants in anisotropic media," Geophysics **79**(5), D349–D362 (2014).
[37]K. Helbig and M. Schoenberg, "Anomalous polarization of elastic waves in transversely isotropic media," J. Acoust. Soc. Am. **81**(5), 1235–1245 (1987).
[38]Z. Koren and I. Ravve, "Slowness domain offset and traveltime approximations in layered vertical transversely isotropic media," Geophys. Prospect. **66**(6), 1070–1096 (2018).
[39]V. Vavryčuk, "Calculation of the slowness vector from the ray vector in anisotropic media," Proc. R. Soc. A: Math. Phys. Eng. Sci. **462**(2067), 883–896 (2006).
[40]H. J. Lee, J. R. Lee, S. H. Moon, T. J. Je, E. C. Jeon, K. Kim, and Y. Y. Kim, "Off-centered double-slit metamaterial for elastic wave polarization anomaly," Sci. Rep. **7**(1), 15378 (2017).
[41]S. I. Ranganathan and M. Ostoja-Starzewski, "Universal elastic anisotropy index," Phys. Rev. Lett. **101**(5), 055504 (2008).
[42]L. Wang, J. Lau, E. L. Thomas, and M. C. Boyce, "Co-continuous composite materials for stiffness, strength, and energy dissipation," Adv. Mater. **23**(13), 1524–1529 (2011).